

Geophysical Research Letters



RESEARCH LETTER

10.1029/2024GL108883

Key Points:

- Relative seismic velocity changes at Axial Seamount show long-term trends reflecting changes in the accommodation of inflation
- Transition in pattern corresponds to change from rapid inflation through uplift to slower inflation through seismic slip of locked faults
- Short-term trends in seismic velocity variation reflect changes in magma supply and pressure with brief periods of deflation events

Supporting Information:

Supporting Information may be found in the online version of this article.

Correspondence to:

M. K. Lee and Y. J. Tan, mlee@ldeo.columbia.edu; yjtan@cuhk.edu.hk

Citation:

Lee, M. K., Tan, Y. J., Russell, J. B., Tolstoy, M., & Waldhauser, F. (2024). Relative seismic velocity variations at Axial Seamount observed with ambient seismic noise capture transition point in volcanic inflation. *Geophysical Research Letters*, *51*, e2024GL108883. https://doi.org/10.1029/2024GL108883

Received 17 FEB 2024 Accepted 24 APR 2024

© 2024. The Authors. This is an open access article under the terms of the Creative Commons Attribution License, which permits use, distribution and reproduction in any medium, provided the original work is properly cited.

Relative Seismic Velocity Variations at Axial Seamount Observed With Ambient Seismic Noise Capture Transition Point in Volcanic Inflation

Michelle K. Lee¹, Yen Joe Tan², Joshua B. Russell³, Maya Tolstoy^{1,4}, and Felix Waldhauser¹

¹Lamont-Doherty Earth Observatory, Columbia University, Palisades, NY, USA, ²Earth and Environmental Sciences Programme, Faculty of Science, The Chinese University of Hong Kong, Hong Kong S.A.R., China, ³Syracuse University, Syracuse, NY, USA, ⁴College of Environment, University of Washington, Seattle, WA, USA

Abstract Temporal changes in seismic velocity estimated from ambient seismic noise can be utilized to infer subsurface properties at volcanic systems. In this study, we process 7 years of continuous seismic noise at Axial Seamount and use cross-correlation functions to calculate the relative seismic velocity changes (dv/v) beneath the caldera. We find a long-term trend of decreasing velocity during rapid inflation, followed by slight increase in velocities as background seismicity increases and inflation rate decreases. Furthermore, we observe small short-term increases in dv/v which coincide with short-term deflation events. Our observations of changes in dv/v and their correlation with other geophysical data provide insights into how the top \sim 1 km of the crust at Axial Seamount changes in response to subsurface magma movement and capture the transition from a period of rapid reinflation to a period where the caldera wall faults become critically stressed and must rupture to accommodate further inflation.

Plain Language Summary Changes in seismic velocity calculated from continuous background seismic signals recorded by seismometers can be used to infer subsurface properties of volcanic systems. In this study, we process 7 years of continuous seismic noise at Axial Seamount, an active submarine volcano, to calculate the relative seismic velocity changes. We find a long-term trend of decreasing velocity during inflation of Axial Seamount, followed by mostly stable relative seismic velocity changes that correlate with an increase in earthquake rate and eventually a decrease in inflation rate. We also observe small short-term increases in relative seismic velocity change which coincide with small short-term deflation events. Our observations of changes in relative seismic velocity change and their correlation to other geophysical data provide insights into how the top \sim 1 km of the crust changes in response to subsurface magma movement and capture a transition in the inflation pattern at Axial Seamount.

1. Introduction

Cross-correlation of seismic ambient noise between two seismometers can be harnessed to detect temporal changes in seismic velocity that provide insight into Earth's subsurface properties and dynamic behavior in the region (e.g., Shapiro & Campillo, 2004). At volcanic systems, the temporal changes in seismic velocity have also been used to monitor volcanic activity (e.g., Bennington et al., 2015; Brenguier et al., 2008; Donaldson et al., 2017, 2019). Seismic studies at subaerial volcanic systems have found evidence for long-term seismic velocity variations related to changing crustal properties during inter-eruptive periods associated with deformation related to magma pressurization (i.e., Brenguier et al., 2008; Donaldson et al., 2017; Duputel et al., 2009). These seismic velocity changes during inter-eruptive periods can provide additional insights into processes beneath a volcano at times between eruptions and can be utilized to understand, and potentially forecast, volcanic eruption processes. However, on land, other natural processes such as temperature, rainfall, and groundwater level changes can also impact seismic velocity (i.e., Bièvre et al., 2018; Guillemot et al., 2021), which complicates the interpretations of seismic velocity variations in relation to magmatic processes. These complexities are not present on the deep seafloor making it an ideal site to study changes in seismic velocity driven by geologic processes.

The area of focus for our study is Axial Seamount, an active submarine volcano located on the Juan de Fuca ridge where it intersects with the Cobb-Eickelberg hot spot. Axial Seamount has had three seismically well-

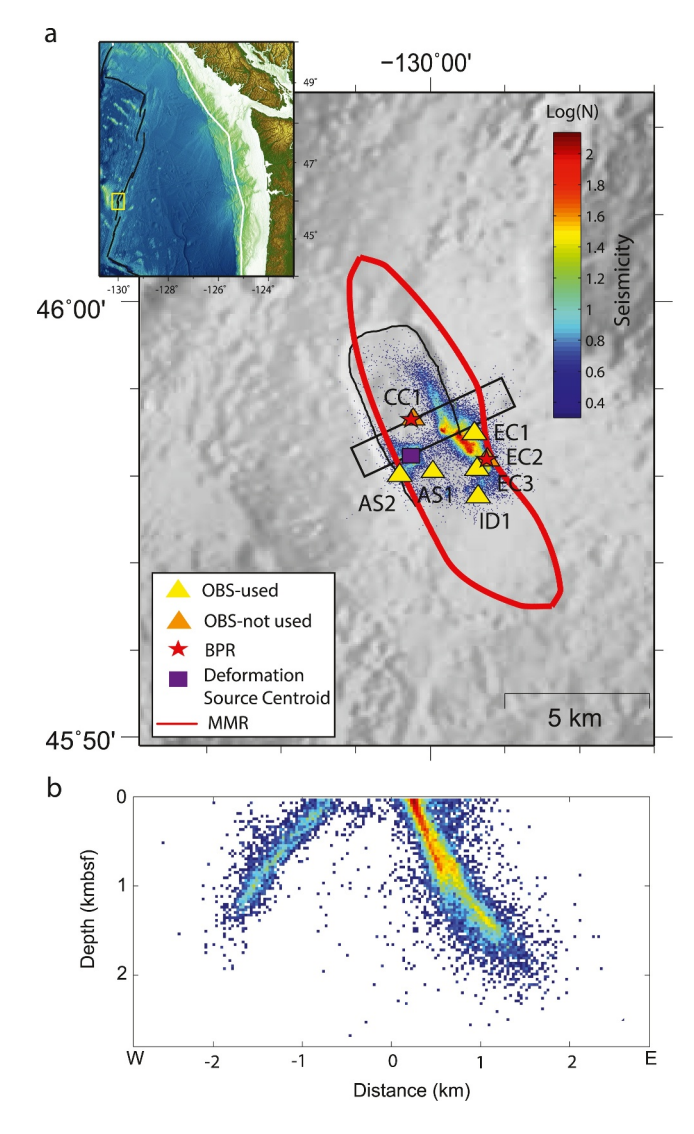


Figure 1. (a) Bathymetric map of Axial Seamount on the Juan de Fuca Ridge. The caldera rim is outlined in black. The triangles indicate locations of the OOI ocean bottom seismometers with labels where yellow and orange indicate OBSs used and not used in this study, respectively. The two red stars indicate the location of the BPR stations. The purple square indicates the centroid of the best-fitting deformation source with net fault-induced deformation removed (Hefner et al., 2020). The main magma reservoir (MMR) (Arnulf et al., 2014, 2018) is also outlined in red. Seismicity from 1 September 2015 until 31 December 2022 is shown as a density distribution with colors indicating logarithmic number of events within bins of 30 × 30 m (from Waldhauser et al. (2020)). Inset shows Juan de Fuca bathymetric map with the geographic extent of Axial Seamount map indicated by the yellow box. (b) Cross-section of location of seismicity with depth adapted from Waldhauser et al. (2020). Location of cross-section indicated by black box in (a).

documented eruptions, with the last one occurring in 2015 (Wilcock et al., 2016, 2018). The main magma reservoir (MMR) beneath Axial Seamount where the eruptions and intrusion events initiated has been imaged using active source seismic techniques to be beneath the central caldera, with a slight offset to the east (Figure 1; Arnulf et al., 2014). Prominent reflections have indicated that the top of the reservoir is located $\sim 1.1-2.3$ km below the seafloor (bsf) with fainter bottom reflections indicating a thickness of 0.6-1 km (Arnulf et al., 2014). Stacked sills have also been located beneath the MMR extending down to ~5 km bsf and can act as a pathway for magma supply into the MMR (Carbotte et al., 2020). The deformation source at Axial Seamount has also been modeled using vertical deformation data and caldera fault motion (Hefner et al., 2020; Nooner & Chadwick, 2016), and is modeled to be a steeply dipping prolate-spheroid located beneath the central western area of the caldera with the center of the spheroid sitting at ~3 kmbsf (Figures 1 and 2). This modeled deformation source matches well with the location of the MMR and stacked sills beneath the center of the summit caldera. Axial Seamount is also a well-monitored location on the deep seafloor, instrumented at present with a variety of sensors, including two broadband and five short-period ocean bottom seismometers (OBS), bottom pressure recorders (BPR), temperature probes, and more, as part of the Ocean Observatory Initiative (OOI)—Regional Cabled Array (RCA) (Kelley et al., 2014) (Figure 1). In contrast to typical free-fall OBS, the OOI OBS are part of an ROV installed cabled network that were carefully installed and buried with good coupling to the seafloor resulting in exceptional data quality. The OOI OBS cabled array has had real-time data streaming since late-2014, providing years of continuous data for long-term ambient noise analysis.

While there have been studies using relative seismic velocity changes to monitor subaerial volcanoes (e.g., Bennington et al., 2015; Brenguier et al., 2008; Donaldson et al., 2017, 2019) and there have been studies that used OBSs to measure relative seismic velocity changes (e.g., Wang et al., 2022), no studies have used OBSs to measure relative seismic velocity changes at submarine volcanoes. In this study, we process ~7 years of data following the 2015 eruption at Axial Seamount to observe seismic velocity changes during the inter-eruptive period to understand the potential crustal structure changes beneath the seamount as it builds up to the next eruption.

2. Methods and Results

We process data from the five short-period OOI OBSs located near and within the caldera of Axial Seamount (Figure 1; Table S1 in Supporting Information S1) starting on 1 September 2015 until 1 January 2023. The two broadband stations were not used due to uncertainties in their instrument response and accurate instrument response corrections would be necessary to process the data with the short-period stations. We utilize the open-source MSNoise software, a python package built to monitor seismic velocity changes using ambient noise analysis techniques (Lecocq et al., 2014). We first preprocess the continuous waveforms by performing one-bit normalization and 30-min window spectral whitening (Bensen et al., 2007). We then

compute cross-correlation functions (CCFs) for every station pair at time lags of ± 120 s that are then stacked for each day. The daily CCFs are then stacked over a 14-day moving window where the 14 days correspond to the days leading up to and including the day (Figure S1 in Supporting Information S1). The reference CCF used for this study is the stacked daily CCFs from January 2016 to January 2023. After calculating the CCFs, the time delays of different arrivals of the coda waves between the CCFs and the reference CCF are measured using the moving-window cross spectrum (MWCS) analysis method with a moving step window of 12 s with 4 s overlap

LEE ET AL. 2 of 8

19448007, 2024, 10, Downloaded from https://agupubs.onlinelibrary.wiley.com/doi/10.1029/2024GL108883 by Columbia University Libraries, Wiley Online Library on [18/05/2024]. See the Terms and Condit

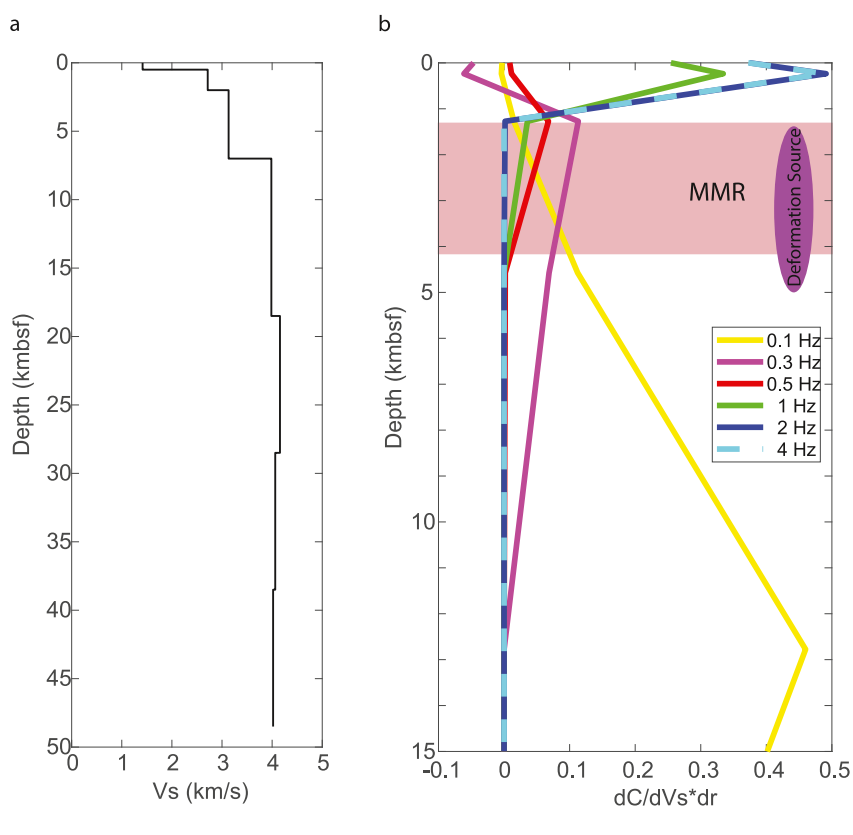


Figure 2. (a) Vs profile used for the sensitivity kernel calculation adapted from Bell et al. (2016) with depth in km below seafloor (kmbsf) (b) Predicted sensitivity kernels as the derivative of the Rayleigh-wave phase velocity with respect to shear velocity multiplied by layer thickness (dC/dVs*dr) for various frequency bands with depth in kmbsf. Depth range of the main magma reservoir (MMR) is labeled and indicated by the red box. Depth range of the modeled deformation source (Hefner et al., 2020) is labeled and marked by a purple spheroid.

(1–2 Hz filter, Table S2 in Supporting Information S1). From the time delays, we only kept the measurements with a coherence greater than 0.65 and an error less than 0.1 s. The relative time shift (dt/t) is then calculated with a weighted linear regression using a 25 s window (1–2 Hz filter, Table S2 and Figure S3 in Supporting Information S1). The minimum time-lag of this window used was determined by dividing the interstation distance by a velocity of 1.0 km/s to exclude the direct arrivals in the CCFs (Figure S4 in Supporting Information S1). The seismic velocity variation is then calculated from dt/t where dv/v = -dt/t with the assumption that dv/v is constant along the path traveled by the signal for each station pair. For this study, we will primarily focus on the results of the average dv/v for all the station pairs. The average dv/v was calculated from a weighted average based on coherence for all the station pairs. The error for calculation of dv/v for each individual station pair and for the average dv/v are estimated from coherence and misfit to the slope from the weighted linear regression on the time delays. When calculating dv/v for a caldera that is inflating and/or deflating, there can be potential uncertainties pertaining to relative station position changes and tilt, however; for our study those effects are negligible relative to the changes we observe in dv/v. Further details on calculating the error and the uncertainties with calculating dv/v are outlined in Text S1 in Supporting Information S1.

For this study, we examine seismic velocity variations using data filtered from 0.1–1 Hz, 1–2 Hz, and 2–4 Hz. Given these selected frequencies and the array's footprint, we expect to primarily sample the upper layer of crust above the identified main magma reservoir (1.1–2.3 km depth with up to 1 km thickness) for the higher frequencies (>0.5 Hz). In order to obtain a rough estimate of sampling depths for these frequencies, we calculate shear-wave sensitivity kernels with the program surf96 (Herrmann, 2013) using a velocity model for the Juan de Fuca plate near Axial Seamount (Figure 2a; Janiszewski et al., 2019; Noguchi et al., 2016). For the starting Rayleigh-wave phase velocity, we used estimates from studies on the Juan de Fuca plate (Janiszewski et al., 2019) for the lower frequencies. For the higher frequencies, no prior studies at the Juan de Fuca plate estimated Rayleigh

LEE ET AL. 3 of 8

a

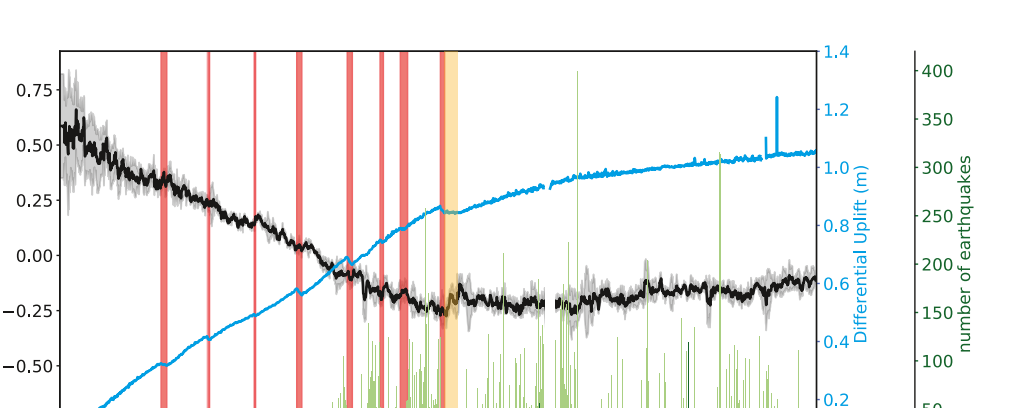
dv/v in %

-0.75

19448007, 2024, 10, Downloaded

from https://agupubs.onlinelibrary.wiley.com/doi/10.1029/2024GL108883 by Columbia University Libraries, Wiley Online Library on [18/05/2024]. See the Terms and Condit

50



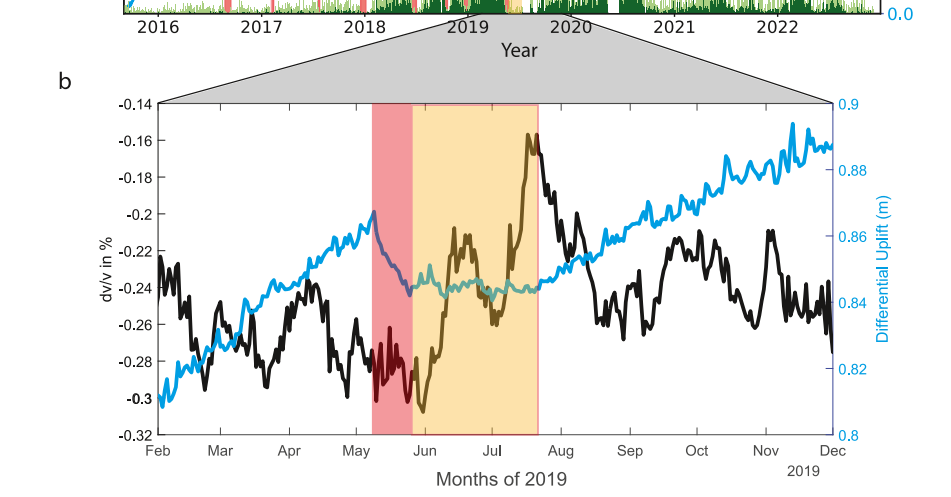


Figure 3. (a) dv/v results for 1–2 Hz filter and 14-day moving window averaged for all station pairs (black) with error (gray) plotted with differential uplift since 1 September 2015 of the de-tided seafloor depth from Central Caldera BPR and Eastern Caldera BPR (blue; data from Chadwick et al. (2022) and OOI) indicating inflation (increase in uplift) and deflation (decrease in uplift) patterns at Axial Seamount and histogram of weekly seismicity rate at Axial (green; data from Wilcock et al., 2016). Light green is the seismicity concentrated on the eastern side of the caldera while dark green is the western side. Red bars indicate timing of short-term deflation events identified by Chadwick et al. (2022). Orange bar indicates the \sim 2-month-long period of no inflation or deflation following the May 2019 short term deflation event. (b) Zoom in plot of dv/v and differential uplift for the May 2019 short-term deflation event (red bar) including the 2-month-long period of no change uplift following the deflation event (orange bar).

phase velocities at these frequencies so we used estimates from a study off the coast of Eastern Japan (Noguchi et al., 2016) for the model section that best corresponded to the structure observed at Axial Seamount. We used the Rayleigh phase velocities derived from the 1-km water depth thickness model of Noguchi et al. (2016) since Axial Seamount is located at 1.4 km below the sea surface. The model also had typical thicknesses for the oceanic crust. From the calculated sensitivity kernels, we estimate that the 1–2 Hz and 2–4 Hz frequency bands are mostly sensitive to the upper 1 km of the oceanic crust. While for the 0.1–1 Hz band, the sensitivity is deeper (Figure 2).

From the relative seismic velocities of the various frequency bands, we observe long-term trends as well as small shorter-term changes. In the 1-2 Hz filtered and the 2-4 Hz filtered data, we observe a long-term decrease in relative seismic velocity until mid-2018 after which the relative seismic velocity changes to a slight long-term increase (Figures 3 and 4; Figure S5 in Supporting Information S1). From 2016 to 2018, the yearly change in dv/v ranges from -0.3% per year to -0.05% per year. The downward trend reverses in 2019 to continue with an increase in dv/v in the range of -0.01%-0.06% per year (Figure 4). In the 0.1-1 Hz filter band, we similarly observe a decreasing long-term pattern that flattens in mid-2018. We additionally observe an annual variation in the relative seismic velocity which is probably an apparent velocity change due to variations in the noise source

LEE ET AL. 4 of 8

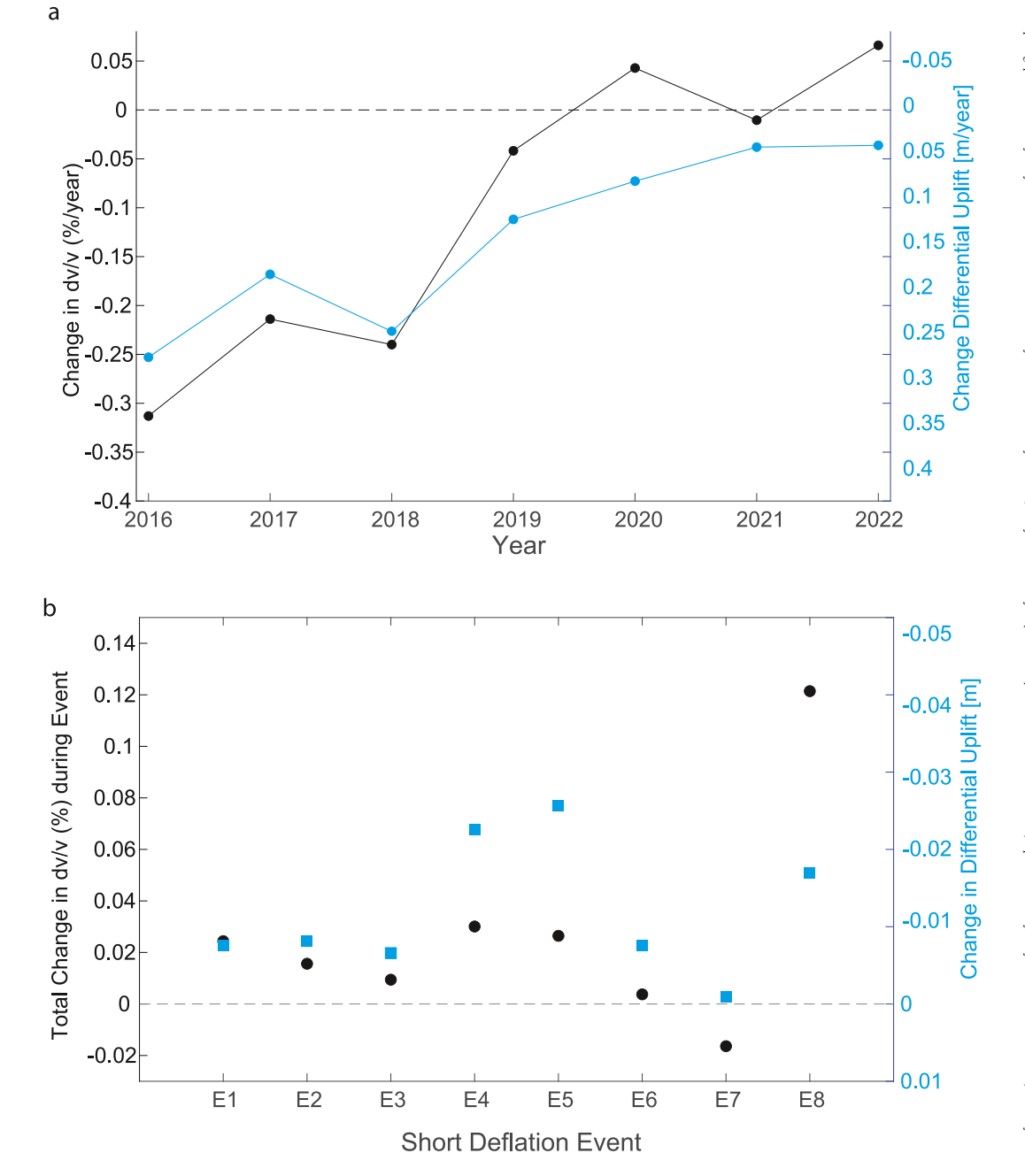


Figure 4. (a) Yearly changes of dv/v (black) and mean differential seafloor depth (blue). (b) Changes of dv/v (black) and mean differential seafloor depth (blue) during each of the 8 short term deflation events indicated as red bars in Figure 3a. Each short-term deflation event is named in order of start date of the event with E1 being the first deflation event that occurred in August 2016 and E8 being the last deflation event that occurred in May 2019. The corresponding name and dates of the short-term deflation events are outlined in Table S2 in Supporting Information S1.

(Figure S5 in Supporting Information S1). In this study, we do not focus on the annual trend observed in the 0.1-1 Hz band, which will be the topic of a future study, but instead focus on the long-term trend that persists across all frequency bands.

3. Discussion

Axial Seamount is a well-studied location that also has long-term data on the inflation-deflation pattern and seismicity dating back to the 1990s. The long-term inflation and deflation pattern of the Axial caldera has also

LEE ET AL. 5 of 8

been recorded through BPR data starting before the 1998 eruption. The inflation-deflation pattern at Axial shows a relatively steady inflation during inter-eruptive periods, with only minor pauses or brief periods of deflation, and a rapid deflation event during the eruption once a certain inflation threshold is met (Nooner & Chadwick, 2016). There is also an extensive real-time seismicity catalog (Waldhauser et al., 2020; Wilcock et al., 2016) for Axial Seamount with earthquakes identified and located from the OBS data of the OOI. Our study is the first to use these OBSs to calculate dv/v to monitor Axial Seamount. In the following section we discuss how the inflation-deflation signal and seismicity patterns correlate with our observed seismic velocity variations.

3.1. Long-Term Trend and Inflation of Axial Caldera

The observed long-term variations in relative seismic velocity highlight the possibility of stress-related changes in cracking and faulting in the upper crust in the years following the 2015 eruption at Axial Seamount. Prior studies using ambient noise to determine variation in seismic velocity at volcanic systems have found a correlation between the changes in seismic velocity with cycles of inflation and deflation due to changes in magma pressurization (i.e., Brenguier et al., 2008; De Plaen et al., 2019; Donaldson et al., 2017; Duputel et al., 2009). A study of the Piton de la Fournaise volcano, from January 2006 to June 2007, by Duputel et al. (2009) observed a decrease in seismic velocity associated with pre-eruptive inflation of the summit. Prior to the July 2006 eruption, when the summit was inflating, they found a decrease in the relative seismicity. They attributed this velocity decrease to the dilation of the medium due to over-pressurization of the magma reservoir and magma migration to the surface with fracture opening. During inflation cracks open causing a decrease in dv/v and during deflation cracks close causing an increase in dv/v.

To assess the observed long-term trend at Axial Seamount, we compare the relative seismic velocity with differential uplift since 1 September 2015 of the de-tided difference in depth between the Central Caldera BPR and the Eastern Caldera BPR (Chadwick et al., 2022) and observe that dv/v is decreasing while the caldera at Axial is inflating, where inflation is defined as an increase in uplift and deflation is defined as a decrease in uplift (Figure 3). When comparing long-term trends yearly we find a strong negative correlation between dv/vand inflation from 2016 to 2019 (Figure 4a). We observe a yearly change in dv/v ranging from -0.05% to -0.3% per year while inflation ranges between 0.25 and 0.5 m/year. Comparing the rate of change of dv/v with inflation pre-2019, we find an inverse linear relationship between dv/v and uplift in that an inflation of 0.1 m approximately corresponds with a decrease of 0.1% in dv/v. We interpret that the decrease in dv/v at Axial Seamount pre-2019 is likely associated with fluid-filled cracks opening from inflation; therefore, reducing seismic velocities, especially those of shear waves. This decrease in dv/v pre-2019 is observed at all station pairs (Figures S6 and S7 in Supporting Information S1) where the magnitude of the decrease from September 2015 until January 2019 is greatest between station pairs that cross through the caldera and smaller between stations along the Eastern caldera wall (Figure S7 in Supporting Information S1). This spatial pattern of dv/vdecrease pre-2019 is broadly consistent with the location of the deformation source at Axial Seamount which results in surface deformation that is greatest within the caldera (Hefner et al., 2020) while the pathways between the Eastern stations are further away from the zone of peak deformation and therefore would show a smaller decrease in dv/v. The correlation between the change in dv/v and inflation pre-2019 suggests that the deformation state and upper crustal velocity structure at Axial are closely interrelated and likely what drives the observed dv/v trend.

Post-2019 the patterns change where with inflation, dv/v is not decreasing but instead is close to constant or slightly increasing. From pre to post-2019, the noise characteristics observed at all the 5 stations do not change significantly between the two time periods (Figure S7 in Supporting Information S1); therefore, the change in pattern is not likely a change in noise characteristics at the stations but reflects some change in the crustal properties. When comparing the timing, this change in dv/v pattern to a constant or slight yearly increase in dv/v (-0.01% to 0.06% per year) is observed around the beginning of 2019 (Figures 3 and 4a) in conjunction with increased seismic activity at Axial Seamount (Figure 3) and coincides with a period when the inflation rate at Axial Seamount declined substantially. Chadwick et al. (2022) reported that the inflation rate started to decrease in late 2018, from 54 cm/year to 48 cm/year by October 2018, and progressively decreased to 7 cm/year by mid-2020. Chadwick et al. (2022) attributed the slower inflation rate to a weakening magma supply and therefore fewer conduits opening for magma transport. While we interpret that pre-2019 the deformation state and upper crustal velocity structure drive the change in dv/v, post-2019 we interpret that due to the slow

LEE ET AL. 6 of 8

inflation rate, the deformation state does not completely drive the observed dv/v changes. In addition to the deformation state, seismic activity provides additional insight into possible mechanisms influencing the relative seismic velocity change at Axial. In the few years after the 2015 eruption when seismicity rate was low, the upper crust's porosity and structure could have been modified by the opening of cracks due to rapid inflation, resulting in a decrease in seismic velocity with fracture opening related to inflation driving the seismic velocity change. Seismicity at Axial Seamount is generally observed to occur along the narrow zones of faulting of the ring fault system (Figure 1, Waldhauser et al., 2020; Wilcock et al., 2016). The ring faults that reach depths of \sim 1.6 km where the top of MMR is located are thought to accommodate stresses caused by inflation (Waldhauser et al., 2020). When seismicity intensified continuously from 2018, it indicates a transition in the mechanism accommodating the inflation, where it has reached a height that the caldera wall faults are critically stressed, and further inflation is accommodated more through seismic slip on the caldera wall rather than rising and doming of the central crust that would open near-surface cracks. We interpret that relatively constant and even slightly increasing yearly change in dv/v is associated with the weak magma supply from the slow inflation being accommodated by the caldera wall faults where seismicity is occurring hence is not accommodated by the opening of cracks across the caldera.

3.2. Increase in dv/v With Small Deflation Events

In addition to the long-term inflation, quasi-periodic short-term deflation events have been identified between August 2016 and May 2019 (Chadwick et al., 2022). Eight discrete short-term deflation events have been identified during that period with each of them lasting 1-3 weeks with a total deflation of about 1-3 cm each time (Table S2 in Supporting Information S1, Figure 3, red bars). At the time of these short-term deflation events, seismicity rate also drops abruptly (Figure 3, green). These short-term deflation events coincide with observed times of slightly increased or relatively constant dv/v (Figure 4b), though the changes are subtle for the smaller events, and may not have been picked out were it not for a clearer association with the May 2019 deflation event where a 2-month long period of no inflation is observed after the deflation event (Figure 3b). The short-term deflation events and the decrease in seismicity may be attributed to a reduction of pressure of the shallow magma reservoir and therefore also a reduction in extensional stress of the crust (Chadwick et al., 2022). Possible mechanisms that could result in the reduction of pressure are the movement of magma out of the reservoir or a pause in magma supply through the sills beneath the reservoir. The reduction of inflationary stresses could result in the closing of shallow cracks and an increase in seismic velocity which we see at the times of short-term deflation events, or times of no inflation. The abrupt drop in seismicity rate is consistent with a brief period where the caldera faults are no longer critically stressed.

4. Conclusions

The seismic velocity changes at Axial Seamount derived from ambient noise analyses between September 2015 to January 2023, reveal long-term and short-term trends. The long-term decrease in seismic velocity from 2015 to early-2019 can be associated with the inflation of the caldera. During inflation, conduits and cracks for fluid and/or magma likely open and increase porosity which would cause a decrease in seismic velocity. During 2019 there is a transition in the seismic velocity to a slight but steady increase of seismic velocities. This transition is likely associated with the transition where deformation is more accommodated by caldera wall fault slip rather than uplift. Within the long-term trend, we also observe short-term increases in seismic velocity coinciding with short-term deflation events which could reflect the closing of cracks during deflation. Our results demonstrated for the first time how ambient seismic noise can be used to track changes in crustal properties at a submarine volcano in response to magma movement.

Data Availability Statement

Data used in this study are archived and publicly available through the Ocean Observatories Initiative (OOI) Data Portal (https://oceanobservatories.org/cabled-array-seismometer-data/) and through Incorporated Research Institutions for Seismology (IRIS) (http://service.iris.edu/irisws/timeseries/1/).

LEE ET AL. 7 of 8

Acknowledgments

We thank the Ocean Observatories Initiative (OOI) and IRIS for the availability and easy accessibility of the seismic data. We thank Bill Chadwick, Scott Nooner, and OOI for sharing their inflation and deflation data and results. We would also like to thank Suzanne Carbotte and Bill Chadwick for insightful discussions. Finally, we would like to thank Alexander Yates and an anonymous reviewer for their comments that helped improve this manuscript. This work was supported by the Croucher Tak Wah Mak Innovation Award and NSF Grant OCE-1834261 and OCE-1951448.

References

- Arnulf, A. F., Harding, A. J., Kent, G. M., & Wilcock, W. S. D. (2018). Structure, seismicity, and accretionary processes at the hot spot-influenced Axial Seamount on the Juan de Fuca Ridge. *Journal of Geophysical Research: Solid Earth*, 123(6), 4618–4646. https://doi.org/10.1029/2017jb015131
- Arnulf, A. F., Singh, S. C., & Pye, J. W. (2014). Seismic evidence of a complex multi-lens melt reservoir beneath the 9°N overlapping spreading center at the East Pacific Rise. *Geophysical Research Letters*, 41(17), 6109–6115. https://doi.org/10.1002/2014GL060859
- Bell, S., Ruan, Y., & Forsyth, D. W. (2016). Ridge asymmetry and deep aqueous alteration at the trench observed from Rayleigh wave tomography of the Juan de Fuca plate. *Journal of Geophysical Research: Solid Earth*, 121(10), 7298–7321. https://doi.org/10.1002/2016JB012990
- Bennington, N. L., Haney, M., Angelis, S. D., Thurber, C. H., & Freymueller, J. (2015). Monitoring changes in seismic velocity related to an ongoing rapid inflation event at Okmok volcano, Alaska. *Journal of Geophysical Research: Solid Earth*, 120(8), 5664–5676. https://doi.org/10.1002/2015JB011939
- Bensen, A., Ritzwoller, M., Barmin, M., Levshin, A., Lin, F., Moschetti, M., et al. (2007). Processing seismic ambient noise data to obtain reliable broad-band surface wave dispersion measurements. *Geophysical Journal International*, 169(3), 1239–1260. https://doi.org/10.1111/j.1365-246X.2007.03374.x
- Bièvre, G., Franz, M., Larose, E., Carrière, S., Jongmans, D., & Jaboyedoff, M. (2018). Influence of environmental parameters on the seismic velocity changes in a clayey mudflow (Pont-Bourquin Landslide, Switzerland). *Engineering Geology*, 245, 248–257. https://doi.org/10.1016/j.enggeo.2018.08.013
- Brenguier, F., Campillo, M., Hadziioannou, C., Shapiro, N. M., Nadeau, R. M., & Larose, E. (2008). Postseismic relaxation along the San Andreas Fault at Parkfield from continuous seismological observations. *Science*, 321(5895), 1478–1481. https://doi.org/10.1126/science.1160943
- Carbotte, S. M., Arnulf, A., Spiegelman, M., Lee, M., Harding, A., Kent, G., et al. (2020). Stacked sills forming a deep melt-mush feeder conduit beneath Axial Seamount. *Geology*, 48(7), 693–697. https://doi.org/10.1130/G47223.1
- Chadwick, W. W., Jr., Wilcock, W. S. D., Nooner, S. L., Beeson, J. W., Sawyer, A. M., & Lau, T.-K. (2022). Geodetic monitoring at Axial Seamount since its 2015 eruption reveals a waning magma supply and tightly linked rates of deformation and seismicity. *Geochemistry, Geophysics, Geosystems*, 23(1), e2021GC010153. https://doi.org/10.1029/2021GC0101533
- De Plaen, R. S. M., Cannata, A., Cannavo, F., Caudron, C., Lecocq, T., & Francis, O. (2019). Temporal changes of seismic velocity caused by volcanic activity at Mt. Etna revealed by the autocorrelation of ambient seismic noise. *Frontiers in Earth Science*, 6, 251. https://doi.org/10.3389/feart.2018.00251
- Donaldson, C., Caudron, C., Green, R. G., Thelen, W. A., & White, R. S. (2017). Relative seismic velocity variations correlate with deformation at Kīlauea volcano. *Science Advances*, 3(6), e1700219. https://doi.org/10.1126/sciadv.1700219
- Donaldson, C., Winder, T., Caudron, C., & White, R. S. (2019). Crustal seismic velocity responds to a magmatic intrusion and seasonal loading in Iceland's Northern Volcanic Zone. Science Advances, 5(11), eaax6642. https://doi.org/10.1126/sciadv.aax6642
- Duputel, Z., Ferrazzini, V., Brenguier, F., Shapiro, N., Campillo, M., & Nercessian, A. (2009). Real time monitoring of relative velocity changes using ambient seismic noise at the Piton de la Fournaise volcano (La Réunion) from January 2006 to June 2007. *Journal of Volcanology and Geothermal Research*, 184(1), 164–173. https://doi.org/10.1016/j.jvolgeores.2008.11.024
- Guillemot, A., van Herwijnen, A., Larose, E., Mayer, S., & Baillet, L. (2021). Effect of snowfall on changes in relative seismic velocity measured by ambient noise correlation. *The Cryosphere*, 15(12), 5805–5817. https://doi.org/10.5194/tc-15-5805-2021
- Hefner, W. L., Nooner, S. L., Chadwick, W. W., Jr., & Bohnenstiehl, D. W. R. (2020). Revised magmatic source models for the 2015 eruption at Axial Seamount including estimates of fault-induced deformation. *Journal of Geophysical Research: Solid Earth*, 125(4), e2020JB019356. https://doi.org/10.1029/2020JB019356
- Herrmann, R. B. (2013). Computer programs in seismology: An evolving tool for instruction and research. Seismological Research Letters, 84(6), 1081–1088. https://doi.org/10.1785/0220110096
- Janiszewski, H. A., Gaherty, J. B., Abers, G. A., Gao, H., & Eilon, Z. C. (2019). Amphibious surface-wave phase-velocity measurements of the Cascadia subduction zone. Geophysical Journal International, 217(3), 1929–1948. https://doi.org/10.1093/gji/ggz051
- Kelley, D. S., Delaney, J. R., & Juniper, S. K. (2014). Establishing a new era of submarine volcanic observatories: Cabling Axial Seamount and the endeavour segment of the Juan de Fuca Ridge. *Marine Geology*, 352, 426–450. https://doi.org/10.1016/j.margeo.2014.03.010
- Lecocq, T., Caudron, C., & Brenguier, F. (2014). MSNoise, a python package for monitoring seismic velocity changes using ambient seismic noise. Seismological Research Letters, 85(3), 715–726. https://doi.org/10.1785/0220130073
- Noguchi, S., Maeda, T., & Furumura, T. (2016). Ocean-influenced Rayleigh waves from outer-rise earthquakes and their effects on durations of long-period ground motion. *Geophysical Journal International*, 205(2), 1099–1107. https://doi.org/10.1093/gji/ggw074
- Nooner, S. L., & Chadwick, W. W. (2016). Inflation-predictable behavior and co-eruption deformation at Axial Seamount. *Science*, 354(6318), 1399–1403. https://doi.org/10.1126/science.aah4666
- Shapiro, N. M., & Campillo, M. (2004). Emergence of broadband Rayleigh waves from correlations of the ambient seismic noise. *Geophysical Research Letters*, 31(7), L07614. https://doi.org/10.1029/2004GL019491
- Waldhauser, F., Wilcock, W. S. D., Tolstoy, M., Baillard, C., Tan, Y. J., & Schaff, D. P. (2020). Precision seismic monitoring and analysis at Axial Seamount using a real-time double-difference system. *Journal of Geophysical Research: Solid Earth*, 125(5), e2019JB018796. https://doi.org/10.1029/2019JB018796
- Wang, W., Savage, M. K., Yates, A., Zal, H. J., Webb, S., Boulton, C., et al. (2022). Temporal velocity variations in the northern Hikurangi margin and the relation to slow slip. Earth and Planetary Science Letters, 584, 117443. https://doi.org/10.1016/j.epsl.2022.117443
- Wilcock, W. S. D., Dziak, R. P., Tolstoy, M., Chadwick, W., Nooner, S., Bohnenstiehl, D. R., et al. (2018). The recent volcanic history of Axial Seamount: Geophysical insights into past eruption dynamics with an eye toward enhanced observations of future eruptions. *Oceanography*, 31(1), 114–123. https://doi.org/10.5670/oceanog.2018.117
- Wilcock, W. S. D., Tolstoy, M., Waldhauser, F., Garcia, C., Tan, Y. J., Bohnenstiehl, D. R., et al. (2016). Seismic constraints on caldera dynamics from the 2015 Axial Seamount eruption. *Science*, 354(6318), 1395–1399. https://doi.org/10.1126/science.aah5563

References From the Supporting Information

Clarke, D., Zaccarelli, L., Shapiro, N. M., & Brenguier, F. (2011). Assessment of resolution and accuracy of the moving window cross spectral technique for monitoring crustal temporal variations using ambient seismic noise. *Geophysical Journal International*, 186(Issue 2), 867–882. https://doi.org/10.1111/j.1365-246X.2011.05074.x

LEE ET AL. 8 of 8